

# A Family of High Order Finite Difference Schemes with Good Spectral Resolution

Krishnan Mahesh

*Center for Turbulence Research, Stanford University, Stanford, California 94305*

E-mail: krishnan@leland.stanford.edu

Received September 19, 1997; revised March 11, 1998

---

This paper presents a family of finite difference schemes for the first and second derivatives of smooth functions. The schemes are Hermitian and symmetric and may be considered a more general version of the standard compact (Padé) schemes discussed by Lele. They are different from the standard Padé schemes, in that the first and second derivatives are evaluated simultaneously. For the same stencil width, the proposed schemes are two orders higher in accuracy, and have significantly better spectral representation. Eigenvalue analysis, and numerical solutions of the one-dimensional advection equation are used to demonstrate the numerical stability of the schemes. The computational cost of computing both derivatives is assessed and shown to be essentially the same as the standard Padé schemes. The proposed schemes appear to be attractive alternatives to the standard Padé schemes for computations of the Navier–Stokes equations. © 1998 Academic Press

---

## 1. INTRODUCTION

Fluid flows in the transitional and turbulent regimes possess a wide range of length and time scales. The numerical computation of these flows therefore requires numerical methods that can accurately represent the entire, or at least a significant portion, of this range of scales. The length scales that are resolved by a computation are determined by the resolution; the accuracy with which these scales are represented depends upon the numerical scheme. Fourier analysis (see, e.g. [2]) describes both the range of scales present and the accuracy with which they are computed (exactly for problems with periodic boundary conditions and in a WKB sense for more general problems). Such analysis of finite difference schemes (see, e.g. Fig. 1 in [1]) shows that the error in computing the first and second derivatives can be quite large for the smaller scales. This small scale inaccuracy becomes increasingly important as the energy in the small scales becomes increasingly comparable to that of the large scales, i.e., as the spectrum becomes increasingly “flat.” This situation is commonly encountered in computations, particularly large-eddy simulations, of high Reynolds number

turbulence. As shown by Kravchenko and Moin [3] the inaccurate numerical representation of the small scales in these large-eddy simulations can result in the numerical error overwhelming the contribution of the subgrid-scale model.

Finite difference schemes may be classified as “explicit” or “implicit.” Explicit schemes express the nodal derivatives as an explicit weighted sum of the nodal values of the function, e.g.,  $f'_i = (f_{i+1} - f_{i-1})/2h$  and  $f''_i = (f_{i+1} - 2f_i + f_{i-1})/h^2$ . Throughout this paper,  $f_i$  and  $f_i^k$  denote the values of the function and its  $k$ th derivative respectively, at the node  $x = x_i$ , and  $h$  denotes the uniform mesh spacing. By comparison, implicit (compact) schemes equate a weighted sum of the nodal derivatives to a weighted sum of the function, e.g.,  $f'_{i-1} + 4f'_i + f'_{i+1} = 3(f_{i+1} - f_{i-1})/h$  and  $f''_{i-1} + 10f''_i + f''_{i+1} = 12(f_{i+1} - 2f_i + f_{i-1})/h^2$ . It is well known [1, 4, 6] that implicit schemes are significantly more accurate for the small scales than explicit schemes with the same stencil width. This increase in accuracy is achieved at the cost of inverting a banded (usually tridiagonal) matrix to obtain the nodal derivatives. Since tridiagonal matrices can be inverted quite efficiently [7], the implicit schemes are extremely attractive when explicit time advancement schemes are used. The most popular of the implicit schemes (also called Padé schemes due to their derivation from Padé approximants) appear to be the symmetric fourth and sixth order versions (see, e.g. [1]). There have been several recent computations of transitional boundary layers [8–11], turbulent flows [12–15], and flow-generated noise [16, 17] that have used the Padé schemes to evaluate the spatial derivatives. The standard Padé schemes are symmetric and therefore nondissipative; a nonsymmetric compact scheme was recently developed by Adams and Shariff [18].

This paper presents a related family of finite difference schemes for the spatial derivatives in the Navier–Stokes equations. The proposed schemes are more accurate than the standard Padé schemes, while incurring essentially the same computational cost. They are based on Hermite interpolation and may be considered a more general version of the standard Padé schemes described in [1]. For the same stencil width as the Padé schemes, the proposed schemes have higher order of accuracy and better spectral representation. This is achieved by simultaneously solving for the first and second derivatives. When defined on a uniform mesh,<sup>1</sup> the schemes are of the form

$$\begin{aligned} a_1 f'_{i-1} + a_0 f'_i + a_2 f'_{i+1} + h(b_1 f''_{i-1} + b_0 f''_i + b_2 f''_{i+1}) \\ = \frac{1}{h}(c_1 f_{i-2} + c_2 f_{i-1} + c_0 f_i + c_3 f_{i+1} + c_4 f_{i+2}). \end{aligned} \quad (1)$$

Note that the above expression differs from the standard Padé schemes, in that the left-hand side contains a linear combination of the first and second derivatives. The stencil and the coefficients are restricted to be symmetric in this paper. The resulting schemes are therefore nondissipative. The width of the stencil is taken to be three on the left-hand side and five on the right. This corresponds to the stencil width of the popular sixth-order Padé scheme.

The motivation to formulate schemes that simultaneously evaluate both derivatives is provided by the Navier–Stokes equations requiring both derivatives of most variables. Consider for example the one-dimensional compressible equations in primitive form (extension

<sup>1</sup> This paper develops the schemes on uniform meshes. It is assumed that computations with nonuniform grids can define analytical mappings between the nonuniform grid and a corresponding uniform grid. The metrics of the mapping may then be used to relate the derivatives on the uniform grid to those on the nonuniform grid.

to multiple dimensions is straightforward). We have

$$\frac{\partial \rho}{\partial t} + u \frac{\partial \rho}{\partial x} = -\rho \frac{\partial u}{\partial x}; \quad (2a)$$

$$\rho \left( \frac{\partial u}{\partial t} + u \frac{\partial u}{\partial x} \right) = -RT \frac{\partial \rho}{\partial x} - R\rho \frac{\partial T}{\partial x} + \underbrace{\frac{4}{3}\mu \frac{\partial^2 u}{\partial x^2} + \frac{4}{3} \frac{\partial u}{\partial x} \frac{d\mu}{dT} \frac{\partial T}{\partial x}}_{\frac{\partial}{\partial x} \left( \frac{4}{3}\mu \frac{\partial u}{\partial x} \right)}; \quad (2b)$$

$$\rho C_v \left( \frac{\partial T}{\partial t} + u \frac{\partial T}{\partial x} \right) = -\rho RT \frac{\partial u}{\partial x} + \frac{4}{3}\mu \left( \frac{\partial u}{\partial x} \right)^2 + \underbrace{k \frac{\partial^2 T}{\partial x^2} + \frac{dk}{dT} \left( \frac{\partial T}{\partial x} \right)^2}_{\frac{\partial}{\partial x} \left( k \frac{\partial T}{\partial x} \right)}. \quad (2c)$$

The variables  $\rho$ ,  $u$ , and  $T$  denote the density, velocity, and temperature, respectively, while  $R$ ,  $\mu$ ,  $k$ , and  $C_v$  denote the specific gas constant, dynamic viscosity, thermal conductivity, and specific heat at constant volume. Note that the viscous terms are expanded prior to their evaluation. This is because direct evaluation of the second derivatives is significantly more accurate at the small scales than two applications of a first derivative operator. Equations (2a)–(2c) show that the following spatial derivatives need to be evaluated:

$$\frac{\partial u}{\partial x}, \frac{\partial^2 u}{\partial x^2}, \frac{\partial T}{\partial x}, \frac{\partial^2 T}{\partial x^2}, \frac{\partial \rho}{\partial x}.$$

Thus, a scheme that simultaneously evaluates both derivatives would only be performing one unnecessary evaluation ( $\partial^2 \rho / \partial x^2$ ).

Next, consider the conservative form of the equations. The viscous terms are evaluated in their nonconservative form for the reasons given above. We have

$$\frac{\partial \rho}{\partial t} + \frac{\partial}{\partial x}(\rho u) = 0; \quad (3a)$$

$$\frac{\partial}{\partial t}(\rho u) + \frac{\partial}{\partial x}(\rho u^2) + \frac{\partial p}{\partial x} = \frac{4}{3}\mu \frac{\partial^2 u}{\partial x^2} + \frac{4}{3} \frac{\partial u}{\partial x} \frac{d\mu}{dT} \frac{\partial T}{\partial x}; \quad (3b)$$

$$\begin{aligned} \frac{\partial E_t}{\partial t} + \frac{\partial}{\partial x}(E_t u) + \frac{\partial}{\partial x}(p u) &= u \left( \frac{4}{3}\mu \frac{\partial^2 u}{\partial x^2} + \frac{4}{3} \frac{\partial u}{\partial x} \frac{d\mu}{dT} \frac{\partial T}{\partial x} \right) \\ &+ \frac{4}{3}\mu \left( \frac{\partial u}{\partial x} \right)^2 + k \frac{\partial^2 T}{\partial x^2} + \frac{dk}{dT} \left( \frac{\partial T}{\partial x} \right)^2. \end{aligned} \quad (3c)$$

Equations (3a)–(3c) require the following spatial derivatives to be obtained:

$$\frac{\partial}{\partial x}(\rho u), \frac{\partial}{\partial x}(\rho u^2), \frac{\partial p}{\partial x}, \frac{\partial u}{\partial x}, \frac{\partial^2 u}{\partial x^2}, \frac{\partial T}{\partial x}, \frac{\partial^2 T}{\partial x^2}, \frac{\partial}{\partial x}(E_t u), \frac{\partial}{\partial x}(p u).$$

As one might expect, the conservative formulation requires fewer simultaneous derivative evaluations. However, if the chain rule is invoked, then a formulation that evaluates both

derivatives is still attractive. First evaluate (simultaneously)

$$\frac{\partial}{\partial x}(\rho u), \frac{\partial^2}{\partial x^2}(\rho u), \frac{\partial}{\partial x}(\rho u^2), \frac{\partial^2}{\partial x^2}(\rho u^2), \frac{\partial \rho}{\partial x},$$

$$\frac{\partial^2 \rho}{\partial x^2}, \frac{\partial}{\partial x}(E_t u), \frac{\partial^2}{\partial x^2}(E_t u), \frac{\partial}{\partial x}(p u), \frac{\partial^2}{\partial x^2}(p u).$$

The chain rule may then be used to obtain  $\partial u/\partial x$ ,  $\partial^2 u/\partial x^2$ ,  $\partial p/\partial x$ , and  $\partial^2 p/\partial x^2$ . The equation of state and the chain rule then yield  $\partial T/\partial x$  and  $\partial^2 T/\partial x^2$ . In this manner, a total of only 10 derivative evaluations are performed for the nine derivatives that are needed. The increase in accuracy that is obtained by the simultaneous evaluation of derivatives will be seen to make this additional derivative evaluation worthwhile.

For the same stencil width, the standard Padé schemes are two orders higher in accuracy and have better spectral representation than the corresponding symmetric, explicit schemes. The implicit relation between the derivatives in the Padé schemes yields additional degrees of freedom that allow higher accuracy to be achieved. It is therefore to be expected that including the second derivatives in the implicit expression would further increase the degrees of freedom and, thereby, the accuracy that can be obtained. Hermitian expressions involving the function and its first and higher derivatives have been suggested in the literature (e.g., [4, Sections 2.4, 2.5]). Peyret and Taylor [19, Section 2.5.1] and Hirsch [20, Section 4.3] discuss a symmetric version of Eq. (1) on a three-point stencil. However, the development was not completed to a point where the resulting schemes could be used for solving partial differential equations.

The objective of this paper is to develop this family of schemes and to assess their potential for computations of the Navier–Stokes equations. The schemes will be referred to as the “coupled-derivative,” or “C-D” schemes, to distinguish them from the standard Padé schemes. The paper is organized as follows. Section 2 describes the interior schemes that may be obtained from Eq. (1). Fourier analysis is then used in Section 3 to perform a detailed comparison between the proposed schemes and the standard Padé schemes. The restrictions imposed by numerical (Cauchy) stability are discussed in Section 4. Section 5 presents appropriate boundary closures for the interior scheme and evaluates the stability of the complete scheme. The computational cost of the proposed schemes is evaluated in Section 6 and compared to that of the standard Padé schemes.

## 2. THE INTERIOR SCHEME

The interior scheme is of the form given by Eq. (1). Simultaneous solving for  $f'_i$  and  $f''_i$  implies that the number of unknowns is equal to  $2N$ . A total of  $2N$  equations are therefore needed to close the system. Equation (1) may be used to derive two linearly independent equations at each node. This is done as follows. Both sides of Eq. (1) are first expanded in a Taylor series. The resulting coefficients are then matched, such that Eq. (1) maintains a certain order of accuracy. Note that Eq. (1) has 11 coefficients, of which one is arbitrary; i.e., Eq. (1) may be divided through by one of the constants without loss of generality. A convenient choice of the normalizing constant is either of  $a_0$  or  $b_0$ . It will be seen that the equation obtained by setting  $a_0$  equal to 1 is linearly independent of the equation obtained when  $b_0$  is set equal to 1. The two equations may therefore be applied at each node, and the resulting system of  $2N$  equations solved for the nodal values of the first and second derivative. The process of obtaining the two equations is outlined in Sections 2.1 and 2.2.

**TABLE I**  
**Taylor Table for  $a_0 = 1$**

LHS	RHS
$f_i$	$0$
$f_i'$	$1 + 2a_1$
$f_i''$	$b_0$
$f_i'''$	$2h^2(a_1/2! + b_2)$
$f_i^{iv}$	$0$
$f_i^v$	$2h^4(a_1/4! + b_2/3!)$
$f_i^{vi}$	$0$
$f_i^{vii}$	$2h^6(a_1/6! + b_2/5!)$
$f_i^{viii}$	$0$
$f_i^{ix}$	$2h^8(a_1/8! + b_2/7!)$

### 2.1. First Equation ( $a_0 = 1$ )

Consider first the case where  $a_0 = 1$ . The symmetry of the schemes requires that  $a_1 = a_2$ ,  $b_1 = -b_2$ ,  $c_1 = -c_4$ , and  $c_2 = -c_3$ . Equation (1) therefore reduces to

$$\begin{aligned} a_1 f_{i-1}' + f_i' + a_1 f_{i+1}' + h(-b_2 f_{i-1}'' + b_0 f_i'' + b_2 f_{i+1}'') \\ = \frac{1}{h} [c_0 f_i + c_3 (f_{i+1} - f_{i-1}) + c_4 (f_{i+2} - f_{i-2})]. \end{aligned} \quad (4)$$

Expanding both sides of Eq. (4) in a Taylor series and collecting terms of the same order yields Table I. Note that ‘‘LHS’’ and ‘‘RHS’’ denote the coefficients of  $f_i^k$  on the left- and right-hand sides, respectively, of Eq. (4).

The Taylor table shows that  $b_0 = c_0 = 0$ . This leaves four undetermined constants ( $a_1$ ,  $b_2$ ,  $c_3$ , and  $c_4$ ). Expressions for these constants may be obtained by matching the terms in the Taylor table. Schemes of order ranging from two through eight may be obtained by solving the resulting set of equations. The coefficients and the resulting orders are listed below.

*Second order.* Matching terms up to  $f_i''$  yields

$$a_1 = -\frac{1}{2} + c_3 + 2c_4, \quad b_2 \text{ arbitrary.} \quad (5a)$$

The resulting leading order error is equal to  $(3 - 12b_2 - 4c_3 + 4c_4)h^2 f_i'''/6$ .

*Fourth order.* Matching terms up to  $f_i^{iv}$  yields

$$a_1 = -\frac{1}{2} + c_3 + 2c_4, \quad b_2 = \frac{1}{12} [3 - 4(c_3 - c_4)]. \quad (5b)$$

The resulting leading order error is given by  $(-15 + 16c_3 + 92c_4)h^4 f_i^v/360$ . Note that  $c_4 = 0$ ,  $c_3 = 3/4$  yield the standard fourth-order Padé scheme for the first derivative.

*Sixth order.* Matching terms up to  $f_i^{vi}$  yields

$$a_1 = \frac{7}{16} - \frac{15}{4}c_4, \quad b_2 = \frac{1}{16}(-1 + 36c_4), \quad c_3 = \frac{15}{16} - \frac{23}{4}c_4. \quad (5c)$$

The resulting leading order error is equal to  $(1/5040 + 3c_4/140)h^6 f_i^{vii}$ . Note that  $c_4 = 1/36$  yields the standard sixth-order Padé scheme for the first derivative.

*Eighth order.* Matching terms up to  $f_i^{viii}$  yields

$$a_1 = \frac{17}{36}, \quad b_2 = -\frac{1}{12}, \quad c_3 = \frac{107}{108}, \quad c_4 = -\frac{1}{108}. \tag{5d}$$

The error to leading order is equal to  $-h^8 f_i^{ix}/90720$ .

Table I shows that  $b_0$  is equal to zero when  $a_0$  is set equal to one. The above expressions may therefore be considered expressions for the nodal values of the first derivative. It also implies that if, instead of setting  $a_0$  equal to one, we set  $b_0$  equal to one, we would obtain an equation that would be linearly independent. The equation thus derived could be considered an expression for the second derivative. This equation is obtained below.

### 2.2. Second Equation ( $b_0 = 1$ )

Consider the case where  $b_0 = 1$ . Note that a tilde is used above the constants to indicate their difference from the constants obtained when  $a_0 = 1$ ; e.g.,  $b_1$  is replaced by  $\tilde{b}_1$ . Symmetry requires that  $\tilde{b}_1 = \tilde{b}_2$ ,  $\tilde{c}_1 = \tilde{c}_4$ ,  $\tilde{c}_2 = \tilde{c}_3$ , and  $\tilde{a}_1 = -\tilde{a}_2$ . Equation (1) therefore becomes

$$\begin{aligned} &\tilde{a}_0 f_i' + \tilde{a}_2 (f_{i+1}' - f_{i-1}') + h(\tilde{b}_1 f_{i-1}'' + f_i'' + \tilde{b}_1 f_{i+1}'') \\ &= \frac{1}{h}[\tilde{c}_1 (f_{i-2} + f_{i+2}) + \tilde{c}_2 (f_{i-1} + f_{i+1}) + \tilde{c}_0 f_i]. \end{aligned} \tag{6}$$

Expanding both sides of the above equation in a Taylor series and collecting terms of the same order yields the Taylor Table II.

Table II shows that  $\tilde{a}_0$  is required to be zero if  $b_0$  is equal to one. The resulting equation may therefore be considered an expression for the second derivative. We have five unknown constants ( $\tilde{c}_0$ ,  $\tilde{c}_1$ ,  $\tilde{c}_2$ ,  $\tilde{a}_2$ , and  $\tilde{b}_1$ ). These constants may be obtained by matching the terms in the above Taylor table and solving the resulting equations. Expressions of varying order are obtained, depending upon the number of equations matched. At first glance, it appears that the order of accuracy obtained ranges from three through nine. By comparison, the expressions obtained when  $a_0$  was equal to 1 ranged from second through eighth order. However,

**TABLE II**  
**Taylor Table for  $b_0 = 1$**

	LHS	RHS
$f_i$	0	$\tilde{c}_0 + 2\tilde{c}_1 + 2\tilde{c}_2$
$f_i'$	$\tilde{a}_0$	0
$f_i''$	$h(2\tilde{a}_2 + 2\tilde{b}_1 + 1)$	$2h(2^2\tilde{c}_1 + \tilde{c}_2)/2!$
$f_i'''$	0	0
$f_i^{iv}$	$2h^3(\tilde{a}_2/3! + \tilde{b}_1/2!)$	$2h^3(2^4\tilde{c}_1 + \tilde{c}_2)/4!$
$f_i^v$	0	0
$f_i^{vi}$	$2h^5(\tilde{a}_2/5! + \tilde{b}_1/4!)$	$2h^5(2^6\tilde{c}_1 + \tilde{c}_2)/6!$
$f_i^{vii}$	0	0
$f_i^{viii}$	$2h^7(\tilde{a}_2/7! + \tilde{b}_1/6!)$	$2h^7(2^8\tilde{c}_1 + \tilde{c}_2)/8!$
$f_i^{ix}$	0	0
$f_i^x$	$2h^9(\tilde{a}_2/9! + \tilde{b}_1/8!)$	$2h^9(2^{10}\tilde{c}_1 + \tilde{c}_2)/10!$

note that the nodal second derivatives in Eq. (1) are premultiplied by  $h$ . Equation (1) (and, therefore, the terms in the Taylor table) needs to be divided through by  $h$  to consider it an expression for the second derivatives. This process will yield expressions for the second derivative, ranging in order from two through eight. The values for the constants and the corresponding orders are given below.

*Second order.* Matching terms up to  $f_i''$  yields

$$\tilde{c}_0 = -2(\tilde{c}_1 + \tilde{c}_2), \quad \tilde{a}_2 = \frac{1}{2}(-1 - 2\tilde{b}_1 + 4\tilde{c}_1 + \tilde{c}_2). \quad (7a)$$

The resulting leading order error is  $(2 - 8\tilde{b}_1 + 8\tilde{c}_1 - \tilde{c}_2)h^2 f_i^{iv}/12$ .

*Fourth order.* Matching terms up to  $f_i^{iv}$  yields

$$\tilde{c}_0 = -2(\tilde{c}_1 + \tilde{c}_2), \quad \tilde{a}_2 = -\frac{3}{4} + \tilde{c}_1 + \frac{5}{8}\tilde{c}_2, \quad \tilde{b}_1 = \frac{1}{4} + \tilde{c}_1 - \frac{\tilde{c}_2}{8}. \quad (7b)$$

The error to leading order is given by  $(-3 + 28\tilde{c}_1 + \tilde{c}_2)h^4 f_i^{vi}/360$ . Note that  $\tilde{c}_1 = 0$ ,  $\tilde{c}_2 = 6/5$  yield the standard fourth-order Padé scheme for the second derivative.

*Sixth order.* Matching terms up to  $f_i^{vi}$  yields

$$\tilde{c}_0 = -6 + 54\tilde{c}_1, \quad \tilde{c}_2 = 3 - 28\tilde{c}_1, \quad \tilde{a}_2 = \frac{9}{8} - \frac{33}{2}\tilde{c}_1, \quad \tilde{b}_1 = -\frac{1}{8} + \frac{9}{2}\tilde{c}_1. \quad (7c)$$

The resulting error to leading order is  $(1/20160 + 3\tilde{c}_1/560)h^6 f_i^{viii}$ . Note that  $\tilde{c}_1 = 3/44$  yields the standard sixth-order Padé scheme for the second derivative.

*Eighth order.* Matching terms up to  $f_i^{viii}$  yields

$$\tilde{c}_0 = -\frac{13}{2}, \quad \tilde{c}_1 = -\frac{1}{108}, \quad \tilde{c}_2 = \frac{88}{27}, \quad \tilde{a}_2 = \frac{23}{18}, \quad \tilde{b}_1 = -\frac{1}{6}. \quad (7d)$$

The resulting leading order error is  $-h^8 f_i^x/453600$ .

### 2.3. The Scheme

The interior scheme involves applying the equations derived in sections 2.1 and 2.2 at each node. The resulting system of  $2N$  equations is then solved to obtain  $f_i'$  and  $f_i''$ . Of the various schemes obtained, two schemes are discussed in detail below. These are the sixth-order scheme with  $c_1 = \tilde{c}_1 = 0$ , and the eighth-order schemes. These schemes have the same stencil width as the standard fourth- and sixth-order Padé schemes. A detailed comparison between these schemes and the standard Padé schemes is therefore performed. The Appendix presents the schemes in matrix form for completeness.

*Sixth-order C-D scheme* ( $c_1 = \tilde{c}_1 = 0$ ).

$$7f'_{i-1} + 16f'_i + 7f'_{i+1} + h(f''_{i-1} - f''_{i+1}) = \frac{15}{h}(f_{i+1} - f_{i-1}). \quad (8a)$$

$$9(f'_{i+1} - f'_{i-1}) - h(f''_{i-1} - 8f''_i + f''_{i+1}) = \frac{24}{h}(f_{i-1} - 2f_i + f_{i+1}). \quad (8b)$$

*Eighth-order C-D scheme.*

$$51f'_{i-1} + 108f'_i + 51f'_{i+1} + 9h(f''_{i-1} - f''_{i+1}) = \frac{107}{h}(f_{i+1} - f_{i-1}) - \frac{f_{i+2} - f_{i-2}}{h}. \quad (9a)$$

$$\begin{aligned} &138(f'_{i+1} - f'_{i-1}) - h(18f''_{i-1} - 108f''_i + 18f''_{i+1}) \\ &= -\frac{f_{i+2} + f_{i-2}}{h} + \frac{352}{h}(f_{i+1} + f_{i-1}) - \frac{702}{h}f_i. \end{aligned} \quad (9b)$$

*Standard fourth-order Padé.*

$$f'_{i-1} + 4f'_i + f'_{i+1} = \frac{3}{h}(f_{i+1} - f_{i-1}). \quad (10a)$$

$$f''_{i-1} + 10f''_i + f''_{i+1} = \frac{12}{h^2}(f_{i-1} - 2f_i + f_{i+1}). \quad (10b)$$

*Standard sixth-order Padé.*

$$f'_{i-1} + 3f'_i + f'_{i+1} = \frac{7}{3h}(f_{i+1} - f_{i-1}) + \frac{f_{i+2} - f_{i-2}}{12h}. \quad (11a)$$

$$2f''_{i-1} + 11f''_i + 2f''_{i+1} = \frac{12}{h^2}(f_{i-1} - 2f_i + f_{i+1}) + \frac{3}{4h^2}(f_{i-2} - 2f_i + f_{i+2}). \quad (11b)$$

The expressions for the first and second derivative are seen to be independent in the standard Padé schemes (Eqs. (10a)–(11b)). Obtaining the first and second derivatives using the standard Padé schemes therefore involves separately inverting two tridiagonal matrices with band length of  $N$ . By comparison, the first and second derivatives are coupled in the C-D schemes. The vector of unknowns is therefore of length  $2N$ ;  $[\cdots f'_{i-1}, f''_{i-1}, f'_i, f''_i, f'_{i+1}, f''_{i+1} \cdots]^T$ . Note that for the same stencil width as the Padé schemes, the C-D schemes are two orders higher in accuracy. This is achieved at the cost of inverting a matrix that has seven bands instead of three. However, although the band width is increased from three to seven, the inversion yields both the first and second derivatives. A more systematic cost comparison with the Padé schemes is performed in Section 6.

### 3. FOURIER ANALYSIS OF THE DIFFERENCING ERROR

Fourier analysis, and the notion of the “modified wavenumber” provides a convenient means of quantifying the error associated with differencing schemes [2]. Consider the test function  $f_j = e^{ikx_j}$  on a periodic domain. Discretize the function on a domain of length  $2\pi$ , using a uniform mesh of  $N$  points. The mesh spacing is therefore given by  $h = 2\pi/N$ . The exact values of the first and second derivative of  $f$  are  $ike^{ikx_j}$  and  $-k^2e^{ikx_j}$ . However, the numerically computed derivatives will be of the form,  $ik'e^{ikx_j}$  and  $-k''^2e^{ikx_j}$ . The variables  $k'$  and  $k''^2$  are functions of  $k$  and  $h$  and are called the modified wavenumber for the first and second derivative operator, respectively. The difference between  $k'$  and  $k$ , and  $k''^2$  and  $k^2$ , provides the differencing error. The modified wavenumbers for the coupled-derivative schemes are derived and compared to the standard Padé schemes in Sections 3.1 and 3.2.



### 3.1. Modified wavenumber for the standard Padé schemes

The modified wavenumbers for the standard Padé schemes are given by Lele [1] as follows.

*First derivative,*

$$k'h = \frac{a \sin kh + b/2 \sin 2kh}{1 + 2\alpha \cos kh}, \quad (12a)$$

where  $\alpha = 1/4$ ,  $a = 3/2$ , and  $b = 0$  for the fourth-order Padé scheme. For the sixth-order Padé scheme,  $\alpha = 1/3$ ,  $a = 14/9$ , and  $b = 1/9$ .

*Second derivative,*

$$k''h^2 = \frac{2a(1 - \cos kh) + b/2(1 - \cos 2kh)}{1 + 2\alpha \cos kh}, \quad (12b)$$

where  $\alpha = 1/10$ ,  $a = 6/5$ , and  $b = 0$  for the fourth-order Padé scheme. For the sixth-order Padé scheme,  $\alpha = 2/11$ ,  $a = 12/11$ , and  $b = 3/11$ .

### 3.2. Modified Wavenumber for the C-D Schemes

The modified wavenumbers for the C-D schemes are given below. As seen in Sections 2.1 and 2.2, the sixth- and eighth-order schemes are members of the following two-equation family of schemes:

$$f'_i + a_1(f'_{i+1} + f'_{i-1}) + hb_2(f''_{i+1} - f''_{i-1}) = \frac{c_3}{h}(f_{i+1} - f_{i-1}) + \frac{c_4}{h}(f_{i+2} - f_{i-2}); \quad (13a)$$

$$\tilde{a}_2(f'_{i+1} - f'_{i-1}) + h(\tilde{b}_1 f''_{i-1} + f''_i + \tilde{b}_1 f''_{i+1}) = \frac{\tilde{c}_0}{h} f_i + \frac{\tilde{c}_2}{h}(f_{i+1} + f_{i-1}) + \frac{\tilde{c}_1}{h}(f_{i+2} + f_{i-2}). \quad (13b)$$

The constants in the above equations are as follows:

*Sixth-order scheme,*

$$c_4 = 0, \quad a_1 = 7/16, \quad b_2 = -1/16, \quad c_3 = 15/16, \quad \tilde{c}_1 = 0, \quad (14)$$

$$\tilde{c}_2 = 3, \quad \tilde{c}_0 = -6, \quad \tilde{a}_2 = 9/8, \quad \tilde{b}_1 = -1/8.$$

*Eighth-order scheme,*

$$c_4 = -1/108, \quad a_1 = 17/36, \quad b_2 = -1/12, \quad c_3 = 107/108, \quad \tilde{c}_1 = -1/108, \quad (15)$$

$$\tilde{c}_2 = 88/27, \quad \tilde{c}_0 = -13/2, \quad \tilde{a}_2 = 23/18, \quad \tilde{b}_1 = -1/6.$$

Equations (13a) and (13b) are used to obtain the modified wavenumbers as follows. Consider the function,  $f_i = e^{ikx_i}$  on a periodic domain. Using the relations,  $f'_{i\pm 1} = f'_i e^{\pm ikh}$  and  $f''_{i\pm 1} = f''_i e^{\pm ikh}$ , Eqs. (13a) and (13b) become

$$f'_i(1 + 2a_1 \cos kh) + f''_i(i2hb_2 \sin kh) = i \frac{2f_i}{h}(c_3 \sin kh + c_4 \sin 2kh); \quad (16a)$$

$$f'_i(i2\tilde{a}_2 \sin kh) + f''_i(h + 2h\tilde{b}_1 \cos kh) = \frac{f_i}{h}(\tilde{c}_0 + 2\tilde{c}_2 \cos kh + 2\tilde{c}_1 \cos 2kh). \quad (16b)$$

Equations (16a) and (16b) may be solved for  $f'_i$  and  $f''_i$ . The resulting expressions are of the form  $ik' f_i$  and  $-k'' f_i$ , where the modified wavenumbers (after some rearrangement) are given by the following expressions:

$$k'h = 2 \sin kh \frac{c_3 + 2c_4\tilde{b}_1 - \tilde{c}_0b_2 + 2(c_3\tilde{b}_1 + c_4 - b_2\tilde{c}_2) \cos kh + 2(c_4\tilde{b}_1 - b_2\tilde{c}_1) \cos 2kh}{1 + 2a_1\tilde{b}_1 + 2\tilde{a}_2b_2 + 2(\tilde{b}_1 + a_1) \cos kh + 2(a_1\tilde{b}_1 - \tilde{a}_2b_2) \cos 2kh}. \tag{17a}$$

$$k''h^2 = -\frac{\tilde{c}_0 + 2a_1\tilde{c}_2 + 2\tilde{a}_2c_3 + 2(\tilde{c}_2 + a_1\tilde{c}_0 + 2\tilde{a}_2c_4) \cos kh}{1 + 2a_1\tilde{b}_1 + 2\tilde{a}_2b_2 + 2(\tilde{b}_1 + a_1) \cos kh + 2(a_1\tilde{b}_1 - \tilde{a}_2b_2) \cos 2kh} - \frac{2(\tilde{c}_1 + a_1\tilde{c}_2 + \tilde{a}_2c_3) \cos 2kh + 4(a_1\tilde{c}_1 - \tilde{a}_2c_4) \cos kh \cos 2kh}{1 + 2a_1\tilde{b}_1 + 2\tilde{a}_2b_2 + 2(\tilde{b}_1 + a_1) \cos kh + 2(a_1\tilde{b}_1 - \tilde{a}_2b_2) \cos 2kh}. \tag{17b}$$

### 3.3. Evaluation of the First Derivative

The modified wavenumbers for the first derivative are shown in Fig. 1. The C-D schemes are seen to follow the exact solution more closely than the standard Padé schemes. Recall that the sixth-order C-D scheme has the same stencil width as the fourth-order Padé, while the eighth-order C-D scheme has the same stencil width as the sixth-order Padé. In spite of its smaller stencil, the sixth-order C-D scheme is seen to have lower error than the sixth-order Padé. A more quantitative comparison of the schemes is provided in Table III. The fractional error in the first derivative may be defined as

$$\epsilon = \frac{|k'h - kh|}{kh}. \tag{18}$$

Figure 1 shows that the error increases as  $kh$  increases. A measure of the accuracy or “resolving ability” of the schemes is therefore provided by specifying a maximum value for  $\epsilon$  and estimating the fraction of the entire range of wavenumbers for which this requirement is met. This quantity is termed the “resolving efficiency” by Lele [1] and is a function of

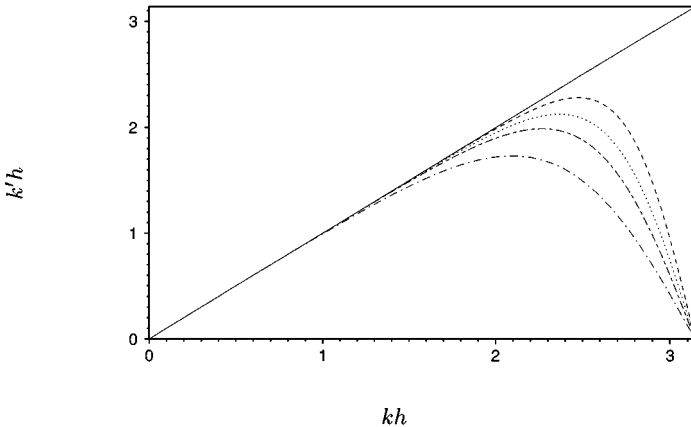


**FIG. 1.** The modified wavenumber for the first derivative. The C-D schemes are compared to the standard Padé schemes: — (exact); ---- (C-D: eighth order); ..... (C-D: sixth order); -.-.- (sixth-order Padé); ——— (fourth-order Padé).

**TABLE III**  
**A Comparison of the Resolving Efficiency**  
**of the C-D Schemes to the Padé Schemes**

	$\epsilon = 0.1$	$\epsilon = 0.01$	$\epsilon = 0.001$
Padé 4	0.59	0.35	0.20
Padé 6	0.70	0.50	0.35
C-D 6	0.75	0.58	0.42
C-D 8	0.81	0.66	0.53

the specified tolerance on the error. Table III compares the resolving efficiency of the C-D schemes to the standard Padé schemes. The C-D schemes are seen to be noticeably more accurate. In fact, of the different compact schemes considered by Lele, the only scheme that outperforms the eighth-order C-D scheme is the pentadiagonal tenth-order scheme (designated “i” by Lele). The pentadiagonal scheme, however, has a stencil of five points on the left-hand side and 7 on the right.

The modified wavenumber may be used to determine the error as a function of the resolution. Consider the case where  $k = 1$ ; i.e., we have one wave of wavelength  $\lambda = 2\pi$ . The mesh spacing  $h$  is given by  $h = 2\pi/N = \lambda/N$ ;  $kh$  is therefore equal to  $\lambda/N$ , the reciprocal of the number of points per wavelength. The percentage error in the first derivative may be computed as a function of the resolution, using  $kh = 2\pi/N$  and  $\text{error} = 100|k'h - kh|/kh$ . Figure 2 compares the C-D schemes to the standard Padé schemes. Note that all the schemes show 100% error for the two-delta waves (two points per wave). This is because the symmetry of the schemes forces  $k'h$  to zero for two-delta waves. The C-D schemes are seen to have noticeably smaller error than the standard Padé schemes. Further indication of this is provided in Fig. 3, where the ratio of the error between the C-D schemes and the Padé schemes is shown. Table IV documents the percentage error in the first derivative for resolutions of 4 and 8 points per wave. The C-D schemes are seen to represent even four delta waves with an accuracy of 0.4% and 0.06%, respectively.

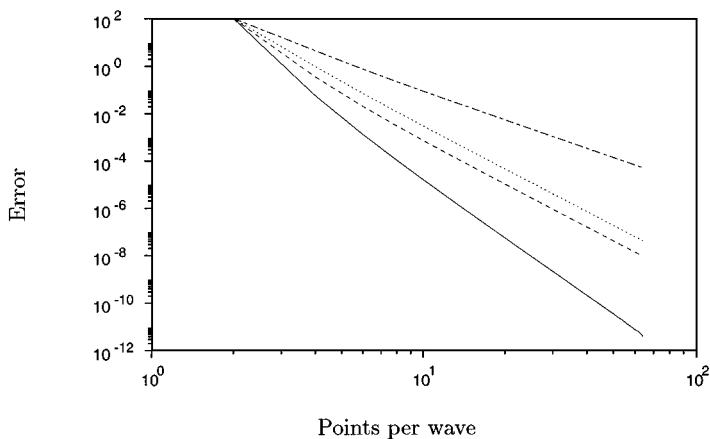


**FIG. 2.** The percentage error in the first derivative as a function of the resolution. The C-D schemes are compared to the standard Padé schemes: — (C-D: eighth order); ---- (C-D: sixth order); ..... (sixth-order Padé); -.-.- (fourth-order Padé).

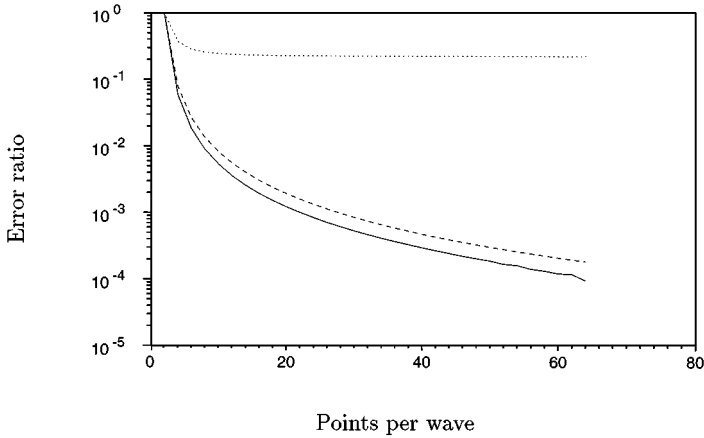


**FIG. 3.** The ratio of the error in the first derivative between the C-D schemes and the standard Padé schemes as a function of the resolution: — (C-D 8/Padé 6); --- (C-D 6/Padé 4); ..... (C-D 6/Padé 6).

### 3.4. Evaluation of Second Derivative

Modified wavenumbers for the second derivative are shown in Fig. 4. The C-D schemes are seen to be noticeably more accurate at the higher wavenumbers. Note that  $k'^2 h^2$  for the C-D schemes is greater than the exact solution for certain wavenumbers. Interestingly, finite element discretizations [5] exhibit similar properties. This is in contrast to the standard Padé schemes, whose modified wavenumber is always less than the exact solution. However, this aspect of the C-D schemes does not impact the accuracy. As shown in Figs. 5 and 6, the C-D schemes are more accurate than the Padé schemes with the same stencil width.

Similar to the first derivative, a resolving efficiency may be defined for the second derivative, as the fraction of the wavenumber range for which the error,

$$\epsilon = \frac{|k'^2 h^2 - k^2 h^2|}{k^2 h^2}, \quad (19)$$

is less than a specified tolerance. The resolving efficiency is tabulated in Table V. Note that the requirement that  $\epsilon$  be less than 0.1 is met over the entire range of wavenumbers. The second derivative computed using the sixth-order C-D scheme is slightly more accurate than the sixth-order Padé scheme, while the eighth-order C-D scheme is noticeably more accurate than the standard Padé schemes. Table VI shows the percentage error in the second

**TABLE IV**  
**The Percentage Error in the First Derivative as a**  
**Function of the Number of Points per Wave ( $N$ )**

	$N = 4$	$N = 8$
Padé 4	4.51%	$2.3 \times 10^{-1}\%$
Padé 6	0.97%	$1.2 \times 10^{-2}\%$
C-D 6	0.36%	$3.1 \times 10^{-3}\%$
C-D 8	0.06%	$1.1 \times 10^{-4}\%$

*Note.* The C-D schemes are compared to the standard Padé schemes.

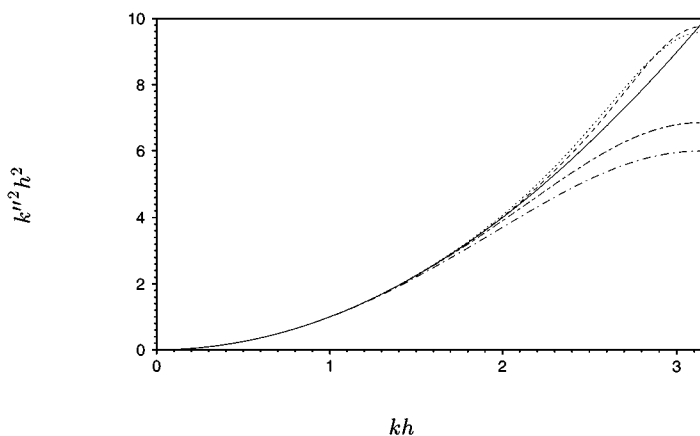


**FIG. 4.** The modified wavenumber for the second derivative. The C-D schemes are compared to the standard Padé schemes: — (Exact); --- (C-D: eighth order); ..... (C-D: sixth order); - - - (sixth-order Padé); - - - (fourth-order Padé).

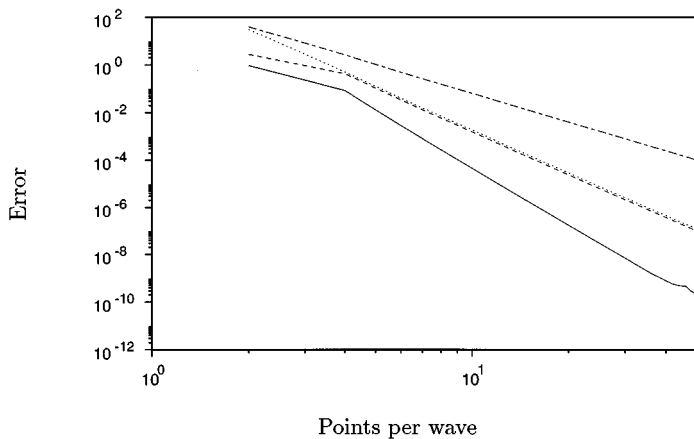


**FIG. 5.** The percentage error in the second derivative as a function of the resolution. The C-D schemes are compared to the standard Padé schemes: — (C-D: eighth order); --- (C-D: sixth order); ..... (sixth-order Padé); - - - (fourth-order Padé).

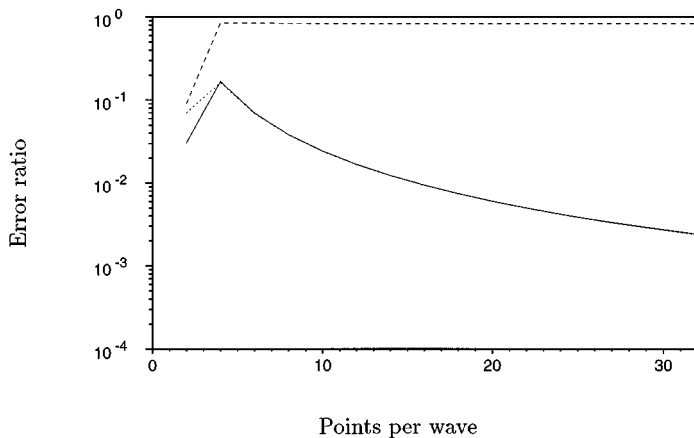


**FIG. 6.** The ratio of the error in the second derivative between the C-D schemes and the standard Padé schemes as a function of the resolution: — (C-D 8/Padé 6); --- (C-D 6/Padé 6); ..... (C-D 6/Padé 4).

**TABLE V**  
**Comparison of Resolving Efficiency of the C-D**  
**Schemes to the Padé Schemes**

	$\epsilon = 0.1$	$\epsilon = 0.01$	$\epsilon = 0.001$
Padé 4	0.68	0.39	0.22
Padé 6	0.80	0.55	0.38
C-D 6	1.00	0.57	0.39
C-D 8	1.00	0.67	0.50

derivative as a function of the resolution. As was observed for the first derivative, the sixth- and eighth-order C-D schemes represent even four-delta waves to an accuracy of about 0.4% and 0.1%, respectively.

#### 4. STABILITY LIMITS OF INTERIOR SCHEME

This section outlines the restrictions imposed by Cauchy stability on the time step when the C-D schemes are used with Runge–Kutta time advancement. The model advection and diffusion equations are solved.

Consider the one-dimensional advection equation on a periodic domain:

$$\frac{\partial u}{\partial t} + c \frac{\partial u}{\partial x} = 0. \quad (20)$$

The above equation is solved by the method of lines. Let  $u = \hat{u} e^{ikx}$ . Spatial discretization leads to a set of ODEs of the form

$$\frac{d\hat{u}}{dt} = -i \frac{c}{h} k' h \hat{u}. \quad (21)$$

The above equation is of the form  $dy/dt = \lambda y$ . It is easily shown that numerical stability requires that

$$\frac{c \Delta t}{h} \leq \frac{(\lambda_i \Delta t)_{\max}}{(k'h)_{\max}}, \quad (22)$$

**TABLE VI**  
**The Percentage Error in the Second Derivative as a**  
**Function of the Number of Points per Wave ( $N$ )**

	$N = 4$	$N = 8$
Padé 4	2.73%	$1.6 \times 10^{-1}\%$
Padé 6	0.52%	$7.41 \times 10^{-3}\%$
C-D 6	0.44%	$6.16 \times 10^{-3}\%$
C-D 8	0.09%	$2.84 \times 10^{-4}\%$

*Note.* The C-D schemes are compared to the standard Padé schemes.

**TABLE VII**  
**The Maximum CFL Number Allowed**  
**by Numerical Stability**

	<i>RK2</i>	<i>RK3</i>	<i>RK4</i>
Padé 4	0	1.0	1.645
Padé 6	0	0.871	1.433
C-D 6	0	0.815	1.341
C-D 8	0	0.759	1.249
Fourier	0	0.551	0.907

where  $(k'h)_{\max}$  denotes the maximum value of the modified wavenumber for the first derivative, and  $(\lambda_i \Delta t)_{\max}$  denotes the upper bound imposed by numerical stability when the ODE  $dy/dt = i\lambda_i y$  is numerically integrated.  $(\lambda_i \Delta t)_{\max}$  has values of 0,  $\sqrt{3}$ , and 2.85 when the standard second-, third-, and fourth-order Runge–Kutta schemes [21] are used for time advancement. Table VII lists the corresponding bounds on the CFL number. As expected, the improved accuracy at the higher wavenumbers reduces the maximum allowable CFL number. Similarly, upper bounds on  $\nu \Delta t/h^2$  can be obtained when the one-dimensional diffusion equation,

$$\frac{\partial u}{\partial t} = \nu \frac{\partial^2 u}{\partial x^2}, \quad (23)$$

is numerically solved on a periodic spatial domain. Table VIII lists the obtained bounds when the C-D schemes are used with Runge–Kutta time advancement. The accuracy of the C-D schemes for the two-delta waves ( $kh = \pi$ ) results in the viscous restriction on the time step being nearly the same as that for a Fourier spectral method.

## 5. BOUNDARY SCHEMES

Consider a spatial domain that is discretized by using  $N$  points (including those at the boundaries). Equations (8a)–(9b) show that the sixth-order scheme can be applied from  $j = 2$  to  $N - 1$ , while the eighth-order scheme can be applied from  $j = 3$  to  $N - 2$ . For problems with periodic boundary conditions, the periodicity of the solution may be used to apply the same equations at the boundary nodes (see the Appendix). However, for non-periodic problems, additional expressions are needed at the boundary nodes to close the system.

**TABLE VIII**  
**The Maximum  $\nu \Delta t/h^2$  Allowed by**  
**Numerical Stability**

	<i>RK2</i>	<i>RK3</i>	<i>RK4</i>
Padé 4	0.333	0.417	0.483
Padé 6	0.292	0.365	0.423
C-D 6	0.208	0.260	0.302
C-D 8	0.205	0.256	0.297
Fourier	0.203	0.253	0.294

Consider  $j = 1$ . The following general expression may be written for  $f'_1$  and  $f''_1$ :

$$a_0 f'_1 + a_1 f'_2 + h(b_0 f''_1 + b_1 f''_2) = \frac{1}{h}(c_1 f_1 + c_2 f_2 + c_3 f_3 + c_4 f_4). \tag{24}$$

The corresponding equation at  $j = N$  would be given by:

$$a_0 f'_N + a_1 f'_{N-1} - h(b_0 f''_N + b_1 f''_{N-1}) = -\frac{1}{h}(c_1 f_N + c_2 f_{N-1} + c_3 f_{N-2} + c_4 f_{N-3}). \tag{25}$$

The width of the stencil on the left-hand side of the above equation is restricted to two. This ensures that the number of bands in the left-hand side matrix is still seven. As was done for the interior scheme, the constants in Eq. (24) may be obtained by expanding the terms in a Taylor’s series and matching expressions of the same order. Recall that we need two independent equations at each node. For the interior schemes, we saw that  $b_0$  was equal to 0 if  $a_0$  was equal to 1 and vice versa. This yielded the two independent equations. As seen from Tables I and II, this relationship between  $a_0$  and  $b_0$  for the interior schemes is a natural consequence of their symmetry. However, for the boundary schemes it turns out that setting  $a_0$  to 1 does not imply that  $b_0$  is zero and vice versa. The equation obtained when  $a_0 = 1$ , is the same as that obtained when  $b_0 = 1$ . The following procedure is therefore used to obtain two independent equations. When matching the terms in the Taylor table,  $(a_0, b_0)$  is first set equal to  $(1, 0)$ . This yields the first equation. Next,  $(a_0, b_0)$  is set equal to  $(0, 1)$ . This yields the second equation. These expressions are derived below.

Taylor’s series expansion of Equation (24) yields Table IX. There are eight undetermined constants in Eq. (1). Note that if either of the constraints  $(a_0, b_0) = (1, 0)$  or  $(0, 1)$  is imposed and the terms in the Taylor table matched, the maximum order that can be obtained is five. The following family of schemes is obtained by matching the the terms in Table IX to different orders. Consider first the case where  $a_0 = 1$  and  $b_0 = 0$ . The resulting expressions may be considered expressions for the first derivative.

5.1. *First Equation* ( $a_0 = 1, b_0 = 0$ )

Expressions for the coefficients and the corresponding orders are given below.

*Third order.* Matching terms up to  $f'''_i$  yields

$$c_1 = -3 + c_3 + 8c_4, \quad c_2 = 3 - 2c_3 - 9c_4, \quad a_1 = 2 - 6c_4, \quad b_1 = -\frac{1}{2} + c_3 + 6c_4. \tag{26a}$$

**TABLE IX**  
**Taylor Table Obtained for the Boundary Schemes**

	LHS	RHS
$f_1$	0	$c_1 + c_2 + c_3 + c_4$
$f'_1$	$a_0 + a_1$	$c_2 + 2c_3 + 3c_4$
$f''_1$	$h(a_1 + b_0 + b_1)$	$h(c_2 + 2^2c_3 + 3^2c_4)/2!$
$f'''_1$	$h^2(a_1/2! + b_1)$	$h^2(c_2 + 2^3c_3 + 3^3c_4)/3!$
$f^{iv}_1$	$h^3(a_1/3! + b_1/2!)$	$h^3(c_2 + 2^4c_3 + 3^4c_4)/4!$
$f^v_1$	$h^4(a_1/4! + b_1/3!)$	$h^4(c_2 + 2^5c_3 + 3^5c_4)/5!$
$f^{vi}_1$	$h^5(a_1/5! + b_1/4!)$	$h^5(c_2 + 2^6c_3 + 3^6c_4)/6!$



The leading order error is then  $(1/24 + c_3/12 + c_4)h^3 f_1^{iv}$ . Note that  $c_3 = 1/2$ ,  $c_4 = 0$  yields the standard one-sided third-order Padé scheme for the first derivative.

*Fourth order.* Matching terms up to  $f_i^{iv}$  yields

$$c_1 = -\frac{7}{2} - 4c_4, \quad c_2 = 4 + 15c_4, \quad c_3 = -\frac{1}{2} - 12c_4, \quad a_1 = 2 - 6c_4, \quad b_1 = -1 - 6c_4. \quad (26b)$$

The error to leading order is given by  $(-1/60 + c_4/5)h^4 f_1^v$ . Note that  $c_4 = -1/6$  yields the standard one-sided fourth-order Padé scheme for the first derivative.

*Fifth order.* Matching terms up to  $f_i^v$  yields

$$c_1 = -\frac{23}{6}, \quad c_2 = \frac{21}{4}, \quad c_3 = -\frac{3}{2}, \quad c_4 = \frac{1}{12}, \quad a_1 = \frac{3}{2}, \quad b_1 = -\frac{3}{2}. \quad (26c)$$

The error to leading order is equal to  $h^5 f_1^{vi} / 120$ .

## 5.2. Second Equation ( $a_0 = 0$ , $b_0 = 1$ )

Similar expressions are obtained when  $a_0 = 0$  and  $b_0 = 1$ . These expressions may be considered relations for the second derivative. The order of the expressions will again range from three to five. However, due to the second derivatives being multiplied by  $h$ , the corresponding order of the second derivatives ranges from two to four. The values of the constants are given below.

*Second order.* Matching terms up to  $f_i'''$  yields

$$c_1 = 6 + c_3 + 8c_4, \quad c_2 = -6 - 2c_3 - 9c_4, \quad a_1 = -6 - 6c_4, \quad b_1 = 2 + c_3 + 6c_4. \quad (27a)$$

The error to leading order is given by  $(-1/4 + c_3/12 + c_4)h^2 f_1^{iv}$ .

*Third order.* Matching terms up to  $f_i^{iv}$  yields

$$c_1 = 9 - 4c_4, \quad c_2 = -12 + 15c_4, \quad c_3 = 3 - 12c_4, \quad a_1 = -6 - 6c_4, \quad b_1 = 5 - 6c_4. \quad (27b)$$

The error to leading order is equal to  $(7/60 + c_4/5)h^3 f_1^v$ . Note that  $c_4 = -1$  yields the standard one-sided third-order Padé scheme for the second derivative.

*Fourth order.* Matching terms up to  $f_i^v$  yields

$$c_1 = 34/3, \quad c_2 = -83/4, \quad c_3 = 10, \quad c_4 = -7/12, \quad a_1 = -5/2, \quad b_1 = 17/2. \quad (27c)$$

The resulting leading order error is given by  $-23h^4 f_1^{vi} / 60$ .

## 5.3. Numerical Stability

The interior schemes outlined in Section 2.3 are combined with the boundary schemes of Sections 5.1 and 5.2 to close the system of equations for the first and second derivatives. Note that the sixth-order interior scheme may be applied from  $j = 2$  to  $j = N - 1$  and, therefore, only needs the boundary expressions at  $j = 1$  and  $N$ . The eighth-order interior scheme uses a five-point stencil on the right-hand side. It therefore can only be applied

from  $j = 3$  to  $N - 2$ . In this paper, if the eighth-order scheme is used in the interior, the system of equations is closed by applying the sixth-order scheme at  $j = 2$  and  $N - 1$ , and the boundary expressions at  $j = 1$  and  $N$ . These expressions are derived below.

Note that the formal order of accuracy of the boundary schemes is less than the interior. This is due to the negative influence of high order (wide stencil) boundary closures on the stability of the overall scheme. Past work has shown that high order boundary closures can result in numerical instability in hyperbolic problems. For example, Carpenter *et al.* [22] compute solutions to the one-dimensional advection equation and show that the standard fourth-order Padé scheme (Eq. (10a)) is asymptotically unstable when the one-sided fourth-order expression

$$f'_1 + 3f'_2 = \frac{1}{6h}(-17f_1 + 9f_2 + 9f_3 - f_4) \tag{28}$$

is used at the boundary nodes. The third-order boundary expression,

$$f'_1 + 2f'_2 = \frac{1}{2h}(-5f_1 + 4f_2 + f_3) \tag{29}$$

is shown to be stable.

The combination of the boundary and interior schemes is numerically integrated to long times, and the solution is examined for boundedness (asymptotic stability). Also, the computational grid is refined while keeping the CFL number fixed, and convergence of the solution established (Lax stability). Details of this evaluation are provided below. Consider the one-dimensional advection equation,

$$\frac{\partial u}{\partial t} + \frac{\partial u}{\partial x} = 0. \tag{30}$$

Equation (30) is numerically solved over the domain  $-1 \leq x \leq 1$ , subject to the following initial and boundary conditions,

$$u(x, 0) = \sin 2\pi x, \quad u(-1, t) = \sin 2\pi(-1 - t). \tag{31}$$

Note that the exact solution to the above equation is given by

$$u_{\text{exact}}(x, t) = \sin 2\pi(x - t). \tag{32}$$

A uniform mesh is used for spatial discretization. The number of grid points (including the boundaries) is set equal to 26, 51, or 101. The solution is then integrated to a time  $t = 100$ . Note that the solution travels one wavelength in one time unit and travels the length of the domain in two time units. The  $L_2$  error,  $\sqrt{1/N \sum_{j=1}^N (u_j - u_{\text{exact}})^2}$ , is then examined for boundedness.

Several combinations of the boundary closures, and the interior scheme were examined. In the following discussion, the notation  $[a, b - c - a, b]$  is used to denote these combinations;  $c$  denotes the order of the interior scheme, while  $a$  and  $b$  denote the order of the expressions for the first and second derivative at  $j = 1$  and  $N$ . For example, the notation  $[3, 3 - 6 - 3, 3]$  implies that the sixth-order scheme (Eqs. (8a), (8b)) is used in the interior, and the third-order equations (26a) and (27b) are used at the boundary nodes. Note that if  $c = 8$ , it is

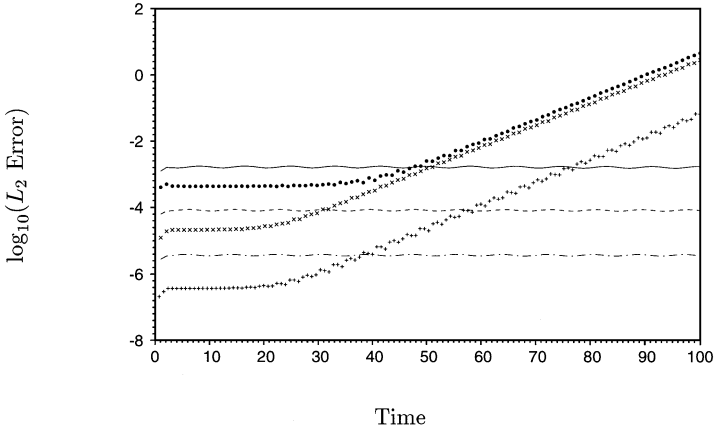


**FIG. 7.** Illustration of the asymptotic instability of the sixth-order C-D scheme with (4, 3) closure at the boundaries. The lines correspond to a  $CFL$  number of 1.33 while the symbols correspond to a  $CFL$  number of 0.1: —, • ( $N = 26$ ); ---, × ( $N = 51$ ); —·—, + ( $N = 101$ ).

implied that the eighth-order scheme is applied from  $j = 3$  to  $N - 2$ , and the sixth-order scheme is applied at  $j = 2$  and  $N - 1$ .

The numerical evaluations show that the stability is essentially dictated by the first derivative expression at the boundary. Schemes involving fourth- and fifth-order expressions for the first derivative, i.e., the schemes [4, 4 - 6 - 4, 4], [4, 3 - 6 - 4, 3], [4, 2 - 6 - 4, 2], [5, 4 - 6 - 5, 4], [5, 3 - 6 - 5, 3], [5, 2 - 6 - 5, 2] were found to be asymptotically unstable. Figure 7 illustrates the observed instability when the [4, 4 - 6 - 4, 4] scheme, i.e. fourth-order boundary closure, along with a sixth-order interior scheme is used. Note that the  $L_2$  error is bounded at the  $CFL$  number of 1.33 (the upper limit for stability of the interior scheme; see Table VII). However, the error is seen to grow exponentially at a smaller  $CFL$  number of 0.1. This behavior is similar to that observed by Carpenter *et al.* [22] when the standard fourth-order Padé scheme (Eq. (10a)) is used along with a fourth-order boundary closure (Eq. (28)). It is a result of the spatial discretization yielding a positive eigenvalue that lies within the stability envelope of the Runge–Kutta scheme at a  $CFL$  number of 1.33.

Similar tests showed that combinations of the third-order expression for the first derivative (Eq. (26a)) with second-, third-, and fourth-order expressions for the second derivative, i.e., the schemes [3, 2 -  $c$  - 3, 2], [3, 3 -  $c$  - 3, 3], [3, 4 -  $c$  - 3, 4] were stable for the sixth- and eighth-order interior schemes. Figure 8 illustrates the stability of the [3, 3 - 6 - 3, 3] scheme.

#### 5.4. Eigenvalue Analysis

Section 5.3 used numerical solutions of the advection equation to identify the boundary closures that yielded stable solutions at long times. An eigenvalue analysis is conducted in this section to confirm that these boundary closures do, indeed, yield asymptotically stable solutions. Consider the advection equation,

$$\frac{\partial u}{\partial t} + c \frac{\partial u}{\partial x} = 0, \quad (33)$$

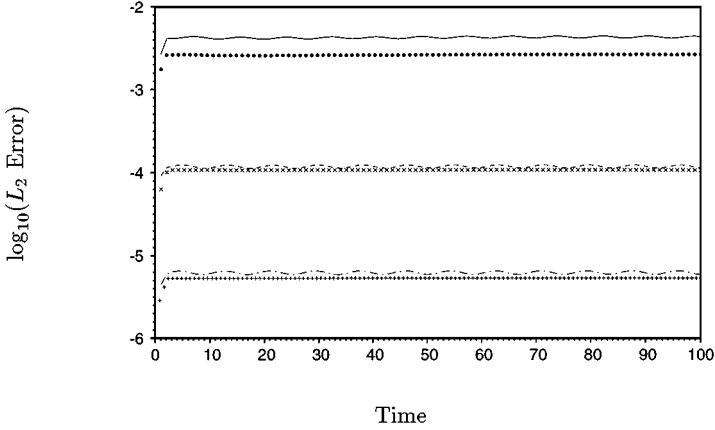


**FIG. 8.** Illustration of the asymptotic stability of the sixth-order C-D scheme with third-order closure at the boundaries. The lines correspond to a  $CFL$  number of 1.33 while the symbols correspond to a  $CFL$  number of 0.1: —, • ( $N = 26$ ); ---, × ( $N = 51$ ); —, + ( $N = 101$ ).

subject to the inflow boundary condition,  $u(0, t) = 0$ .<sup>2</sup> Discretize  $u$  on a uniform grid of  $N$  points (including the boundaries). The inflow condition implies that  $u_1(t) = 0$ . Equation (33) is therefore solved for  $u_j$ , where  $j$  varies from 2 to  $N$ . Spatial discretization yields a set of ODEs of the form

$$\frac{du_j}{dt} = \frac{c}{h} M_{jk} f_k, \quad (34)$$

where  $j$  and  $k$  vary from 2 to  $N$ .  $\mathbf{M}$  is a  $N - 1$  by  $N - 1$  matrix and is defined such that  $u'_j = -M_{jk} u_k$ . The eigenvalues of  $\mathbf{M}$  determine the asymptotic stability of the system of ODEs. The requirement that the eigenvalues of  $\mathbf{M}$  have negative real parts ensures asymptotic stability. The matrix  $\mathbf{M}$  is obtained as follows. First, the condition  $u_1 = 0$ ; the boundary expressions, and the interior scheme are used to eliminate  $u'_1$  and  $u''_1$  from the system of equations for the nodal derivatives. The resulting system of equations is then rearranged as follows. Recall that we use two independent equations relating  $u'_j$  and  $u''_j$  at each node. It is easily seen that these two equations may be expressed in the form

$$\mathbf{A}\mathbf{u}' + h\mathbf{B}\mathbf{u}'' = \frac{1}{h}\mathbf{R}_1\mathbf{u}, \quad (35a)$$

$$\mathbf{C}\mathbf{u}' + h\mathbf{D}\mathbf{u}'' = \frac{1}{h}\mathbf{R}_2\mathbf{u}. \quad (35b)$$

Note that the above system of equations is applied at the nodes  $j = 2$  to  $N$ .  $\mathbf{u}''$  may be eliminated from the above system of equations to obtain an expression relating  $\mathbf{u}'$  to  $\mathbf{u}$ . Premultiplying Eqs. (35a) and (35b) by  $\mathbf{B}^{-1}$  and  $\mathbf{D}^{-1}$ , respectively, and subtracting yields

$$(\mathbf{B}^{-1}\mathbf{A} - \mathbf{D}^{-1}\mathbf{C})\mathbf{u}' = \frac{1}{h}(\mathbf{B}^{-1}\mathbf{R}_1 - \mathbf{D}^{-1}\mathbf{R}_2)\mathbf{u}, \quad (36)$$

<sup>2</sup> This simple inflow condition is adequate to determine the inherent stability of the system. A more general inflow condition,  $u(0, t) = g(t)$ , would simply yield a forcing term on the right-hand side of Eq. (34). The stability of the system would still be governed by the eigenvalues of  $\mathbf{M}$ .

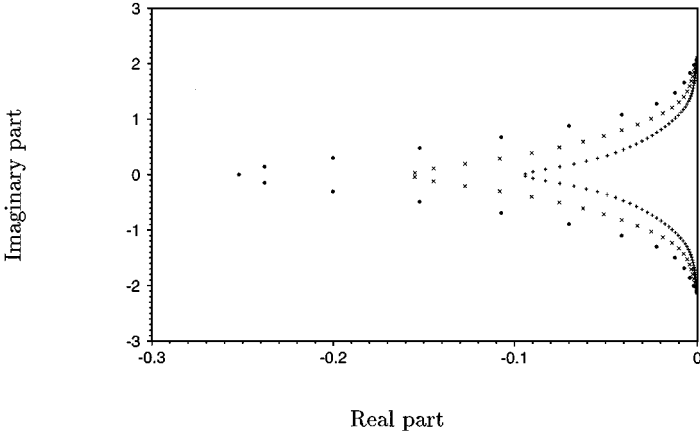


**FIG. 9.** Eigenvalues obtained when the (3, 3) closure is used along with the sixth-order interior scheme:  $\bullet$  ( $N = 26$ );  $\times$  ( $N = 51$ );  $+$  ( $N = 101$ ).

implying that

$$\mathbf{f}' = -\frac{1}{h}(\mathbf{B}^{-1}\mathbf{A} - \mathbf{D}^{-1}\mathbf{C})^{-1}(\mathbf{B}^{-1}\mathbf{R}_1 - \mathbf{D}^{-1}\mathbf{R}_2)\mathbf{f}. \tag{37}$$

Comparison to the relation  $u'_j = -M_{jk}u_k$  yields the expression for  $\mathbf{M}$ :

$$\mathbf{M} = (\mathbf{B}^{-1}\mathbf{A} - \mathbf{D}^{-1}\mathbf{C})^{-1}(\mathbf{B}^{-1}\mathbf{R}_1 - \mathbf{D}^{-1}\mathbf{R}_2). \tag{38}$$

The stability of the (3, 2), (3, 3), and (3, 4) boundary closures (Sections 5.1, 5.2) was tested for both sixth- and eighth-order interior schemes. The number of points  $N$  was set equal to 26, 51, or 101. The matrices  $\mathbf{A}$ ,  $\mathbf{B}$ ,  $\mathbf{C}$ ,  $\mathbf{D}$ ,  $\mathbf{R}_1$ , and  $\mathbf{R}_2$  were specified, and Eq. (38) was used to (numerically) obtain  $\mathbf{M}$ . An eigenvalue solver from the IMSL library was then used to obtain the eigenvalues of  $\mathbf{M}$ . All three boundary closures were found to yield eigenvalues with negative real parts. Figures 9 and 10 illustrate the eigenvalues obtained when the (3, 3) closure was used with the sixth- and eighth-order interior schemes, respectively.

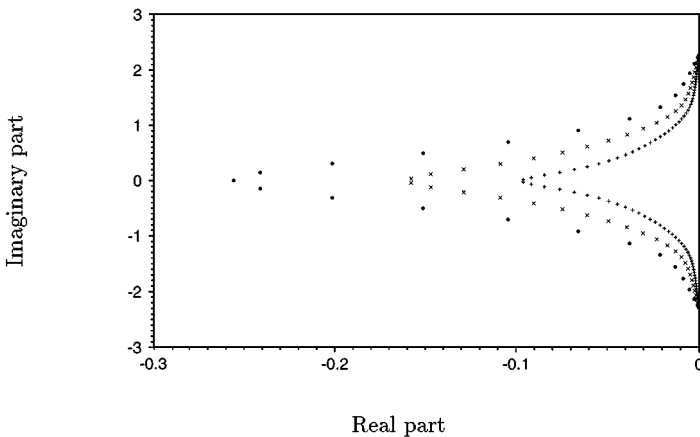


**FIG. 10.** Eigenvalues obtained when the (3, 3) closure is used along with the eighth order interior scheme:  $\bullet$  ( $N = 26$ );  $\times$  ( $N = 51$ );  $+$  ( $N = 101$ ).

### 5.5. The Stable Boundary Closures

The stable boundary closures are summarized below. The following expressions are used at  $j = 1$ . Equation (25) may be used to obtain the corresponding expressions at  $j = N$ . Also, note that lower order boundary schemes reduce the formal order of the overall scheme to one greater than that of the boundary [13].

(3, 4) *boundary closure*. The third-order expression for the first derivative is combined with a fourth-order expression for the second derivative:

$$f'_1 + 2f'_2 - \frac{h}{2}f''_2 = \frac{3}{h}(f_2 - f_1), \quad (39a)$$

$$-\frac{5}{2}f'_2 + h\left(f''_1 + \frac{17}{2}f''_2\right) = \frac{1}{h}\left(\frac{34}{3}f_1 - \frac{83}{4}f_2 + 10f_3 - \frac{7}{12}f_4\right). \quad (39b)$$

(3, 3) *boundary closure*. The third-order expression for the first derivative is combined with a third-order expression for the second derivative:

$$f'_1 + 2f'_2 - \frac{h}{2}f''_2 = \frac{3}{h}(f_2 - f_1), \quad (40a)$$

$$-6f'_2 + h(f''_1 + 5f''_2) = \frac{3}{h}(3f_1 - 4f_2 + f_3). \quad (40b)$$

(3, 2) *boundary closure*. The third-order expression for the first derivative is combined with a second-order expression for the second derivative:

$$f'_1 + 2f'_2 - \frac{h}{2}f''_2 = \frac{3}{h}(f_2 - f_1), \quad (41a)$$

$$-6f'_2 + h(f''_1 + 2f''_2) = \frac{6}{h}(f_1 - f_2). \quad (41b)$$

The matrix form of the schemes obtained with the (3, 3) closure is provided in the Appendix for completeness.

## 6. COST COMPARISON

The computational cost of the C-D schemes is compared to that of the standard Padé schemes in this section. The standard Padé schemes and the C-D schemes are both of the form

$$\mathbf{A}\tilde{\mathbf{f}} = \mathbf{B}\mathbf{f}, \quad (42)$$

where  $\mathbf{f} = [\dots f_{i-1}, f_i, f_{i+1}, \dots]^T$  and  $\mathbf{A}$  and  $\mathbf{B}$  are constant matrices that depend on the scheme. For the standard Padé schemes, the vector  $\tilde{\mathbf{f}}$  is of length  $N$  and is either equal to  $[\dots f'_{i-1}, f'_i, f'_{i+1}, \dots]^T$  or  $[\dots f''_{i-1}, f''_i, f''_{i+1}, \dots]^T$ . Also, the matrix  $\mathbf{A}$  is tridiagonal with a bandlength of  $N$ . For the C-D schemes,  $\tilde{\mathbf{f}}$  is of length  $2N$  and is equal to  $[\dots f'_{i-1}, f''_{i-1}, f'_i, f''_i, f'_{i+1}, f''_{i+1}, \dots]^T$ . The matrix  $\mathbf{A}$  now has seven bands (see the Appendix), each of length equal to  $2N$ .

**TABLE X**  
**The Operation Count per Node to Compute the**  
**First and Second Derivatives**

	<i>RHS</i>	<i>LU</i> solve	Total
Padé 4	1 + 1, 2 + 2	3 + 2, 3 + 2	16
Padé 6	2 + 3, 3 + 4	3 + 2, 3 + 2	22
C-D 6	3 + 3	14 + 12	32
C-D 8	3 + 7	14 + 12	36

*Note.* The entries are of the form, “number of multiples + adds/subtracts.” The comma in the Padé entries separates the cost for the first and second derivatives.

At first glance, it might appear as if the C-D schemes would be significantly more expensive. However, this is not the case. Although the matrix bandwidth and the solution vector length of the C-D schemes is twice that of the standard schemes, a single evaluation yields both first and second derivatives. When the cost of computing both derivatives is estimated, the C-D schemes are seen to incur essentially the same cost as the standard Padé schemes. This is illustrated below. In using schemes of the form given by Eq. (42), the common practice is to perform *LU* decomposition of the matrix **A** only once and store the *L* and *U* matrices. Computation of the derivatives therefore involves computing the right-hand side (**Bf**), followed by forward and back substitution. The operation count associated with computing the right-hand side and solving the resulting system of equations is tabulated in Table X. When the cost of computing both derivatives is estimated, the C-D schemes are seen to involve at most factor of 2 more operations. As shown below, this increase in the number of operations is not very significant.

A cost evaluation was performed on a CRAY C90, using LAPACK routines for the *LU* decomposition and the solution of the *LU* decomposed system. The LAPACK routines took advantage of the banded structure of the coefficient matrix. The function  $f = \sin(x)$  was discretized using a uniform mesh of 128 points on a domain of length equal to  $2\pi$ . Individual routines computed the right-hand side, generated and *LU* decomposed the matrix **A**, and solved the system of equations. Each of these procedures was performed 1000 times, and the result was averaged to determine the cost per evaluation. The cost in microseconds is listed in Table XI. The C-D schemes are seen to incur essentially the same cost as the standard Padé schemes when the cost of computing both derivatives is considered.

**TABLE XI**  
**The Time in Microseconds to Compute Both First**  
**and Second Derivatives on a Mesh of 128 Points**

	<i>LU</i> decomposition	<i>RHS</i>	<i>LU</i> solve
Padé 4	1575	3.6	462
Padé 6	1577	5.2	462
C-D 6	1620	2.6	404
C-D 8	1840	3.8	416

*Note.* All computations use LAPACK routines for banded matrices on a CRAY C90 in vector mode.









4. L. Collatz, *The Numerical Treatment of Differential Equations* (Springer-Verlag, New York, 1966).
5. P. M. Gresho and R. L. Sani, *Incompressible Flow and the Finite Element Method* (Wiley, New York, 1997).
6. Z. Kopal, *Numerical Analysis* (Wiley, New York, 1961).
7. G. Strang, *Linear Algebra and Its Applications* (Harcourt Brace Jovanovich, San Diego, 1988).
8. C. D. Pruett and T. Zang, Direct numerical simulation of laminar breakdown in high-speed, axisymmetric boundary layers, *Theor. Comput. Fluid Dyn.* **3**, 345 (1992).
9. C. D. Pruett, T. Zang, C.-L. Chang, and M. H. Carpenter, Spatial direct numerical simulation of high-speed, boundary layer flows. Part I. Algorithmic considerations and validation, *Theor. Comput. Fluid Dyn.* **7**, 49 (1995).
10. C. D. Pruett and C.-L. Chang, Spatial direct numerical simulation of high-speed, boundary layer flows. Part II. Transition on a cone in Mach 8 flow, *Theor. Comput. Fluid Dyn.* **7**, 397 (1995).
11. N. A. Adams and L. Kleiser, Subharmonic transition to turbulence in a flat plate boundary layer at Mach 4.5, *J. Fluid Mech.* **317**, 301 (1996).
12. Y. Guo and N. A. Adams, Numerical investigation of supersonic turbulent boundary layers with high wall temperature, in *Proceedings, 1994 Summer Program, Center for Turbulence Research, Stanford University*.
13. B. Gustafsson, The convergence rate for difference approximations to mixed initial boundary value problems, *Math. Comp.* **29**, 396 (1975).
14. S. Lee, S. K. Lele, and P. Moin, Direct numerical simulation of isotropic turbulence interacting with a weak shock wave, *J. Fluid Mech.* **251**, 533 (1993).
15. K. Mahesh, S. K. Lele, and P. Moin, *The Interaction of a Shock Wave with a Turbulent Shear Flow*, Report No. TF-69, Thermosciences Division, Mech. Engrg., Stanford University (1996).
16. T. Colonius, P. Moin, and S. K. Lele, *Direct Computation of Aerodynamic Sound*, Report No. TF-65, Thermosciences Division, Mech. Engrg., Stanford University (1995).
17. B. E. Mitchell, S. K. Lele, and P. Moin, *Direct Computation of the Sound Generated by Subsonic and Supersonic Axisymmetric Jets*, Report No. TF-66, Thermosciences Division, Mech. Engrg., Stanford University (1995).
18. N. A. Adams and K. Shariff, *A High-Resolution Hybrid Compact-ENO Scheme for Shock-Turbulence Interaction Problems*, CTR Manuscript 155, Center for Turbulence Research, Stanford University, 1995.
19. R. Peyret and T. D. Taylor, *Computational Methods for Fluid Flow* (Springer-Verlag, New York, 1983).
20. C. Hirsch, *Numerical Computation of Internal and External Flows. Volume 1. Fundamentals of Numerical Discretization* (Wiley, New York, 1988).
21. C. W. Gear, *Numerical Initial Value Problems in Ordinary Differential Equations* (Prentice-Hall, Englewood Cliffs, NJ, 1971).
22. M. H. Carpenter, D. Gottlieb, and S. Abarbanel, Stable and accurate boundary treatments for compact, high-order finite-difference schemes, *Appl. Num. Math.* **12**, 55 (1993).